

# Heisenberg scaling of imaging resolution by coherent enhancement

Robert McConnell,<sup>1,\*</sup> Guang Hao Low,<sup>2</sup> Theodore J. Yoder,<sup>2</sup> Colin D. Bruzewicz,<sup>1</sup> Isaac L. Chuang,<sup>2</sup> John Chiaverini,<sup>1</sup> and Jeremy M. Sage<sup>1</sup>

<sup>1</sup>*Lincoln Laboratory, Massachusetts Institute of Technology, Lexington, Massachusetts 02420, USA*

<sup>2</sup>*Massachusetts Institute of Technology, Cambridge, Massachusetts 02139, USA*

(Dated: June 8, 2016)

Classical imaging works by scattering photons from an object to be imaged, and achieves resolution scaling as  $1/\sqrt{t}$ , with  $t$  the imaging time. By contrast, the laws of quantum mechanics allow one to utilize quantum coherence to obtain imaging resolution that can scale as  $1/t$  – the so-called “Heisenberg limit.” However, ambiguities in the obtained signal often preclude taking full advantage of this quantum enhancement, while imaging techniques designed to be unambiguous often lose this optimal Heisenberg scaling. Here, we demonstrate an imaging technique which combines unambiguous detection of the target with Heisenberg scaling of the resolution. We also demonstrate a binary search algorithm which can efficiently locate a coherent target using the technique, resolving a target trapped ion to within 3% of the  $1/e^2$  diameter of the excitation beam.

Imaging is an essential task in many areas of science, from biology to astronomy to condensed matter physics. Classically, imaging is performed by illuminating a target and collecting those photons which scatter from it. The scale of imaging resolution in this case is set by the wavelength  $\lambda$  of the imaging light and the numerical aperture of the imaging system, but the resolution improves only as the square root of the number of scattered photons and hence as the square root of imaging time  $t$ . Especially in situations when the numerical aperture of the imaging system is limited, the practically-achievable resolution can be insufficient to resolve details of interest.

Numerous imaging techniques which outperform the traditional diffraction limit have been demonstrated [1–4]. These techniques typically work by “excluding” targets not within a sub-diffraction-limited area by storing such targets in a non-scattering, “dark” state  $|d\rangle$ , then scattering imaging photons off of remaining targets in a bright state  $|g\rangle$  on a strong transition  $|g\rangle \rightarrow |e\rangle$ . While these techniques have realized resolution as low as  $\lambda/10$  in some cases [5, 6], they are still limited to a classical time scaling of  $1/\sqrt{t}$  because they do not utilize the full quantum mechanical coherence of their targets.

By contrast, the coherent properties of a quantum mechanical two-level system in principle allow resolution scaling at the so-called Heisenberg limit, as  $1/t$  [7, 8]. A single spin precessing under a Hamiltonian  $H$  accumulates phase  $\phi = (H/\hbar)t$  and a single measurement of this phase achieves resolution  $\Delta\phi = \pi/2$  [9]. If the particle position  $x$  can be linearly mapped to  $H$ , positional uncertainty  $\Delta x \sim \Delta\phi/t$  scaling as  $1/t$  can be achieved.

Realizing such resolution is difficult, though, because of ambiguities in the determination of the phase  $\phi$ . For example, one common way to utilize phase information is to map the phase to an observable such as the probability

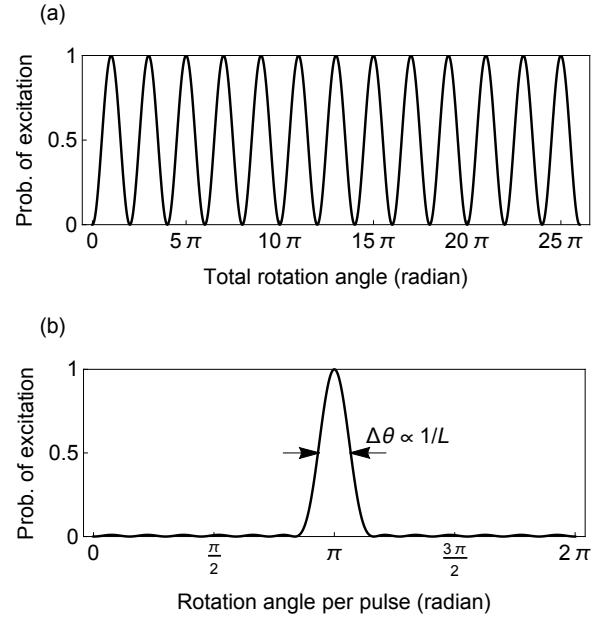


FIG. 1. (a) Coherent oscillations in a driven two level system produce very narrow features which in principle can be used to achieve Heisenberg-limited resolution, but signal ambiguities often preclude achieving such resolution in practice. (b) A sequence of  $L$  pulses of the same overall duration as the drive in (a) can produce an unambiguous single excitation peak whose width nevertheless preserves optimal Heisenberg scaling as  $1/L$ , by varying the phases  $\phi_i$  of each pulse. Here,  $L = 13$ .

to transfer the target to an excited state  $|e\rangle$  (Figure 1). However, when a single long pulse is used (Figure 1(a)), other phases separated by a multiple of  $2\pi$  from the correct phase can lead to identical observables, which can render a precise estimation of the actual phase impossible. Techniques to produce unambiguous phase mappings [10–12] often do so at the expense of Heisenberg scaling, returning to a classical scaling  $\sim 1/\sqrt{t}$ .

In this proof-of-principle experiment, we demonstrate

\* robert.mcconnell@ll.mit.edu

an imaging technique which exploits quantum mechanical coherence and optimal quantum control to unambiguously resolve a trapped atomic ion with Heisenberg scaling of the resolution. Optimally-designed pulse sequences [13] transfer the target ion from its ground state  $|g\rangle$  to excited state  $|e\rangle$  with a position uncertainty scaling as  $1/L$ , with  $L$  the length of the pulse sequence (Figure 1(b)). By using a binary search algorithm which starts with broad excitation and progressively narrows, we efficiently determine the ion position to within 3% of the control beam diameter. To our knowledge, this represents the first experiment to approach Heisenberg-limited scaling in an imaging task. This technique has applications both in traditional imaging and in site-selective addressing of coherent targets within an array [14–16]. The technique is related to, and may complement, methods to increase the frequency resolution of quantum sensors [17, 18].

Our quantum-enhanced imaging technique requires a coherent drive coupling the target states  $|g\rangle, |e\rangle$  with a Rabi frequency  $\Omega$  and able to implement arbitrary rotations on the Bloch sphere of an angle  $\theta = \Omega t$ . Quantum-enhanced imaging is implemented by a sequence of  $L$  such rotations. Within such a sequence, each pulse is performed for the same time  $t_0$  and with the same laser intensity such that the rotation angle  $\theta$  per pulse is the same. However, the phase  $\phi_i$  of each pulse  $i$  in the sequence is optimized such that the ion is only transferred from  $|g\rangle$  to  $|e\rangle$  if the rotation per pulse satisfies  $\theta = \pi$  to within an error  $\Delta\theta \sim 1/L$  (Figure 1(b)). We here consider a 1-D case, but this technique can readily be generalized to higher dimensions.

The Heisenberg-limited scaling of the error in rotation angle  $\theta$  can be mapped to position resolution by using the spatially-varying intensity of a Gaussian beam. In particular, the ion Rabi frequency as a function of position obeys

$$\Omega(x) = \Omega_0 e^{-x^2/w^2}, \quad (1)$$

where  $w$  is the beam waist ( $1/e^2$  intensity radius) and  $\Omega_0$  the ion Rabi frequency at the center of the beam. The positional mapping is optimized if the excitation occurs at the location of maximum field slope of the beam, that is, if  $\Omega(x)t_0 = \pi$  for the point where  $|d\Omega/dx|$  is maximized. This maximum occurs when the beam intensity and pulse length  $t_0$  are chosen such that  $\Omega_0 t_0 = \pi\sqrt{e}$ . For this  $\Omega_0$ , and at the location of maximum slope  $x = w/\sqrt{2}$ , the positional error  $\Delta x$  obeys

$$\Delta x = \frac{\Delta\theta \cdot w}{\pi\sqrt{2}}. \quad (2)$$

The phases that produce such a narrowband excitation are described in [13, 19] and are derived from Chebyshev polynomials. In essence, these pulse sequences trade small probabilities of excitation (“ripples”) in the stopband for an optimally narrow passband, in analogy to Chebyshev filters (c.f. Figure 1(b)).

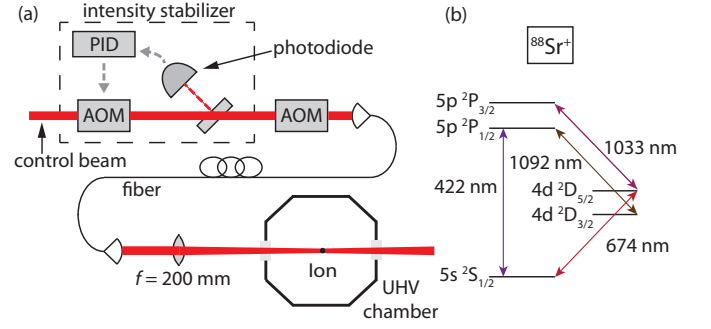


FIG. 2. (a) Schematic of the apparatus used to perform quantum-enhanced imaging. The 674 nm control beam passes through an intensity stabilization circuit (described in text) and then an AOM used to control its intensity. The beam passes through a fiber and then enters the apparatus, where it is focused onto the ion. PID = proportional-integral-differential feedback controller. (b) Relevant level structure in  $^{88}\text{Sr}^+$ .

Figure 2 shows the apparatus we use to perform quantum-enhanced imaging, described in greater detail in [20]. A trapped  $^{88}\text{Sr}^+$  ion is confined  $50\ \mu\text{m}$  above the surface of a Nb surface electrode trap cooled to 4 K via a vibrationally-isolated cryocooler. The ion is coherently driven on the 674 nm,  $|g\rangle = |5S_{1/2}, m = -1/2\rangle \rightarrow |e\rangle = |4D_{5/2}, m = -5/2\rangle$  quadrupole transition with lifetime  $\sim 0.5$  s. Approximately 3 mW of power from a diode laser locked to an ultrastable cavity provide a Rabi frequency of typically  $\Omega_0 = 2\pi \times 100$  kHz. In order to limit intensity fluctuations of the control laser at the ion location, we use a home-built intensity stabilization circuit. A photodiode samples a portion of the beam power; this photodiode signal is sent to a proportional-integral-differential feedback controller which adjusts the modulation input of an acousto-optical modulator (AOM) to maintain constant power. After the intensity stabilizer, we use a second AOM to modulate the power of the control beam at the ion location. Finally, this output passes through a single-mode fiber and emerges from a fiber launch near the experiment which minimizes angular jitter of the beam. This output is focused on the ion by a lens of focal length 200 mm. By adjusting the lens position with a manual micrometer and measuring the change in ion Rabi frequency with position, we determine the control laser beam waist to be  $140 \pm 10\ \mu\text{m}$  at the ion location. These measurements also confirm the Gaussian shape of the control beam.

High-fidelity readout of the ion’s internal state is accomplished by collecting light scattered by a 422 nm laser resonant with the strong  $5S_{1/2} \rightarrow 5P_{1/2}$  transition which couples only to  $|g\rangle$  and not to  $|e\rangle$ . Additional repumping lasers at 1092 nm and 1033 nm prevent population trapping in undesired internal states of the ion.

Figure 3 shows the results of applying excitation pulse sequences of varying length to the trapped ion. With the

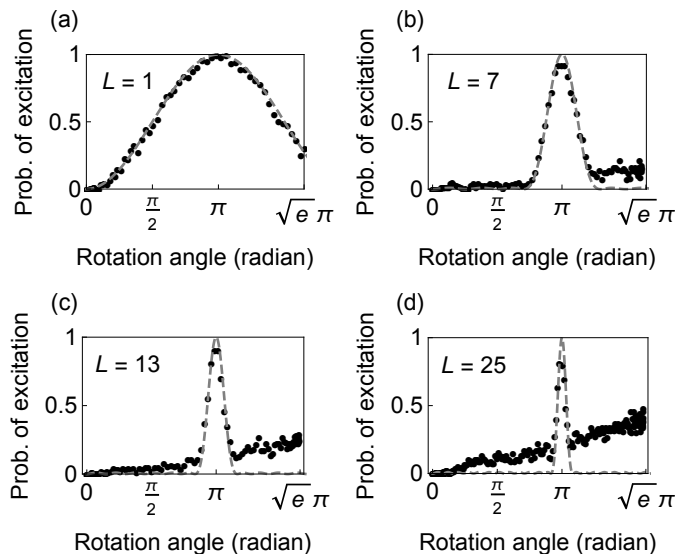


FIG. 3. Examples of quantum-enhanced imaging for (a) a single pulse, (b) a 7-pulse sequence, (c) a 13-pulse sequence, (d) a 25-pulse sequence. The dashed curves show model-free theory predictions for the excitation as a function of drive strength.

ion initially in  $|g\rangle$ , a pulse sequence of length  $L$  and per-pulse rotation angle  $\theta$  is applied; afterwards, we measure the final state of the ion. We perform 200 repetitions per point in order to estimate the probability of the transition  $|g\rangle \rightarrow |e\rangle$  for each  $L$  and  $\theta$ . For the experiments shown in Figure 3, the ion is located at the center of the beam and the beam intensity adjusted via the control AOM. Figure 3(a) shows a single pulse applied to the ion, in which case a broad excitation  $|g\rangle \rightarrow |e\rangle$  occurs which does not well localize the ion. As the number of pulses is increased (Figure 3(b)-(d)), a narrow and unambiguous excitation is achieved. The dashed curves in the figure show the theoretical transfer probability; we demonstrate excitation widths that are in very good agreement with the theoretical predictions.

As the sequence length  $L$  is increased, a noise background begins to appear which reduces the discrimination ability of the sequence. This background is due to spectral noise of the 674 nm control laser which remains unfiltered due to the finite bandwidth of our feedback loop. We have successfully modeled the observed noise background via a simulation that numerically propagates a Hamiltonian with two components: a narrow resonant drive and a 1-MHz broad, incoherent background at a level  $\sim 30$  dB below the main peak; this spectrum agrees with spectrum analyzer measurements of the laser noise. In future work, using the ultrastable cavity as a filter [21] may improve our ability to realize very long, error-free pulse sequences. Despite this background, we are able to resolve the narrow excitation peak for sequences as long as  $L = 53$  pulses, for which we achieve rotation

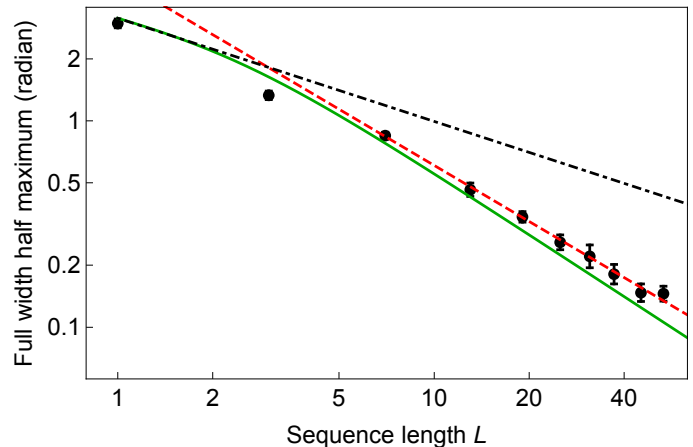


FIG. 4. Scaling of the FWHM of the excitation region as a function of pulse sequence length  $L$ . The solid green curve shows the theoretical width that should be achieved (asymptotically scaling as  $1/L$ ), while the dashed red curve shows a power-law fit to all points for  $L \geq 7$  which finds scaling as  $L^{-0.90 \pm 0.02}$ . The black dot-dashed curve shows classical scaling as  $L^{-0.5}$ .

angle resolution  $(\Delta\theta)/(2\pi) = 0.023 \pm 0.003$ .

Figure 4 shows the scaling of the fitted full width half maximum (FWHM) of the peaks in the experimental data as a function of sequence length  $L$ . The green curve shows the theoretical prediction, while the dashed red curve shows a power law fit to all points for  $L \geq 7$ . The power law fit shows scaling of  $L^{-0.90 \pm 0.02}$ , well beyond the classical  $L^{-0.5}$  scaling (black dash-dotted curve) and approaching the Heisenberg scaling of  $L^{-1}$ . The small deviation from  $L^{-1}$  is due to slight broadening of the excitation peaks due to the spectral noise of the laser (described above).

Finally, we demonstrate a binary search technique to locate an ion of an initially unknown location (Figure 5). The essence of the binary search is as follows. An ion of initially unknown location is addressed by the coherent control beam. For convenience we assume the ion is in the half-space  $x > 0$  for which the ion Rabi frequency  $\Omega(x) \propto e^{-x^2/w^2}$  is monotonically decreasing; thus, an unambiguous mapping between position  $x$  and local Rabi frequency  $\Omega(x)$  exists. (Relaxing this requirement would necessitate only one additional, short measurement to determine whether the ion was in the positive or negative half-space of the beam and would thus have negligible impact on the total imaging time.) A short sequence of length  $L_1$  is initially applied to the ion. The initial search space is divided into a small number  $M$  of different locations identified by position  $x_k$ ; at each location  $x_k$  we perform  $n$  repetitions of the pulse sequence to attempt to drive the ion to  $|e\rangle$ . If the number of successful excitations of the ion out of  $n$  repetitions exceeds a user-specified threshold  $T$  at one of the  $M$  locations and at no others, the ion is considered to be found at that loca-

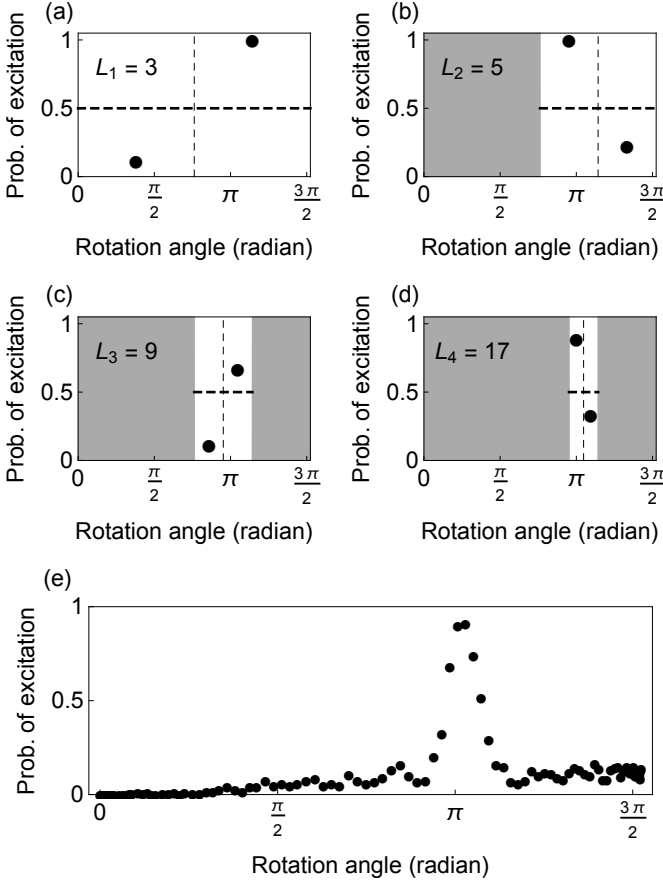


FIG. 5. Demonstration of the logarithmic search technique. The beam is positioned so that its maximum intensity slope is located at the ion position. (a) - (d) Successive pulse sequences of length  $L_1 = 3$ ,  $L_2 = 5$ ,  $L_3 = 9$ ,  $L_4 = 17$  pulses are used to excite the ion. The amplitude is varied to determine the regions where the ion is excited. A threshold of  $T = 0.5$  (dashed horizontal line) is used. Only  $M = 9$  repetitions need be used for each scan due to the unambiguous, narrow feature inherent to the excitation sequences. With each iteration, searched locations where the ion was not found can be excluded (gray regions), the ion position is further localized, and subsequent pulse sequences search only in the remaining target area. (e) A full scan with the 17-pulse sequence reveals the position of the ion, in agreement with the result of the logarithmic search technique.

tion. This localizes the ion to the position  $x_k$  to within an error  $\Delta x_1 \propto 1/L_1$ . The length of the sequence is then increased to  $L_2$ , and the resulting subspace of size  $\Delta x_1$  is then itself divided into  $M$  search locations. This process is repeated, each iteration  $i$  localizing the ion to a corresponding  $\Delta x_i \propto 1/L_i$  until the final  $\Delta x_f$  is less than some specified uncertainty goal.

Rather than physically moving our control beam, we instead vary its intensity and search for the amplitude  $\Omega_{\text{target}}$  such that  $\Omega_{\text{target}} e^{-x^2/w^2} t_0 = \pi$ . We choose the ion position  $x = w/\sqrt{2}$  to maximize the intensity gradi-

ent, and hence positional resolution, of our beam. The results are shown in Figure 5. We use  $M = 2$  searches per iteration of the sequence,  $n = 9$  repetitions per search location, a threshold  $T = 0.5$ , and proceed from the  $L_1 = 3$  pulse sequence to the  $L_4 = 17$  pulse sequence to localize the ion. Once we have finished four iterations of this procedure, the ion is localized to within a rotation angle uncertainty  $(\Delta\theta)/(2\pi) = 0.048$ . Figure 5(e) shows a thorough positional search with the 17-pulse sequence which verifies that the binary search has indeed correctly located the ion. Given our beam waist of  $140 \pm 10 \mu\text{m}$ , the spatial resolution we achieve via binary search corresponds to positional error  $\Delta x = 9 \pm 1 \mu\text{m}$ , or an error of  $3.2 \pm 0.3\%$  of the  $1/e^2$  beam diameter of  $280 \mu\text{m}$ .

In conclusion, we have demonstrated a new method of imaging which takes advantage of quantum coherence to achieve Heisenberg-limited scaling of the resolution. In our proof-of-principle experiment, we have achieved positional resolution to within 3% of the beam diameter, and are able to perform even longer sequences which excite the ion with rotational angle uncertainty  $(\Delta\theta)/(2\pi) = 0.023$ . This is, to our knowledge, the first experiment to approach Heisenberg scaling of the resolution in an imaging task. The technique has many possible uses in traditional imaging applications, especially for longer wavelengths (e.g., microwaves) where the size of the imaging beam may be large compared to details of interest. Furthermore, the selective excitation provided by these pulse sequences may be useful for site-selective control of trapped ions or other quantum systems, such as quantum dots or nitrogen vacancy centers. As one example, a very narrow pulse may be used to drive a target rotation in a particular qubit in an array while minimizing crosstalk effects on other nearby qubits. While technical noise prevents us from achieving sub-wavelength resolution in this proof-of-principle experiment, a sequence of length  $L \approx 270$  pulses would achieve such resolution for our beam waist and may be achievable with improvements to the laser lock system.

We thank Peter Murphy and Chris Thourmaraj for assistance with ion trap chip packaging. This work was sponsored by the National Reconnaissance Office (NRO) and performed under Air Force Contract #FA8721-05-C-0002. Opinions, interpretations, conclusions, and recommendations are those of the authors and are not necessarily endorsed by the United States Government.

- 
- [1] M. Hofmann, C. Eggeling, S. Jakobs, and S. W. Hell, Proceedings of the National Academy of Sciences of the United States of America **102**, 17565 (2005).
  - [2] M. J. Rust, M. Bates, and X. Zhuang, Nature Methods **3**, 793 (2006).
  - [3] E. Betzig, G. H. Patterson, R. Sougrat, O. W. Lindwasser, S. Olenych, J. S. Bonifacino, M. W. Davidson,

- J. Lippincott-Schwartz, and H. F. Hess, *Science* **313**, 1642 (2006).
- [4] A. S. Trifonov, J.-C. Jaskula, C. Teulon, D. R. Glenn, N. Bar-Gill, and R. L. Walsworth, in *Advances in Atomic, Molecular, and Optical Physics*, Advances In Atomic, Molecular, and Optical Physics, Vol. 62, edited by P. R. B. Ennio Arimondo and C. C. Lin (Academic Press, 2013) pp. 279 – 302.
- [5] E. Betzig and J. K. Trautman, *Science* **257**, 189 (1992).
- [6] S. W. Hell, *Science* **316**, 1153 (2007).
- [7] V. Giovannetti, S. Lloyd, and L. Maccone, *Science* **306**, 1330 (2004).
- [8] R. Demkowicz-Dobrzanski, J. Kolodynski, and M. Guta, *Nature Communications* **3**, 1063 (2012).
- [9] N. F. Ramsey, *Phys. Rev.* **78**, 695 (1950).
- [10] N. V. Vitanov, *Phys. Rev. A* **84**, 065404 (2011).
- [11] J. A. Jones, *Phys. Rev. A* **87**, 052317 (2013).
- [12] G. H. Low, T. J. Yoder, and I. L. Chuang, *Phys. Rev. A* **89**, 022341 (2014).
- [13] G. H. Low, T. J. Yoder, and I. L. Chuang, *Phys. Rev. Lett.* **114**, 100801 (2015).
- [14] D. J. Wineland, C. Monroe, W. M. Itano, D. Leibfried, B. E. King, and D. M. Meekhof, *J. Res. Natl. Inst. Stand. Technol.* **103**, 259 (1998).
- [15] C. Shen, Z.-X. Gong, and L.-M. Duan, *Phys. Rev. A* **88**, 052325 (2013).
- [16] J. T. Merrill, S. C. Doret, G. Vittorini, J. P. Addison, and K. R. Brown, *Phys. Rev. A* **90**, 040301 (2014).
- [17] K. Arai, C. Belthangady, H. Zhang, N. Bar-Gill, S. DeVience, P. Cappellaro, A. Yacoby, and R. Walsworth, *Nature Nanotechnology* **10**, 859 (2015).
- [18] J. Sastrawan, C. Jones, I. Akhalwaya, H. Uys, and M. J. Biercuk, arXiv:1407.3902v2 [quant-ph] (2016).
- [19] G. H. Low, T. J. Yoder, and I. L. Chuang, arXiv:1603.03996v1 [quant-ph] (2016).
- [20] J. M. Sage, A. J. Kerman, and J. Chiaverini, *Phys. Rev. A* **86**, 013417 (2012).
- [21] N. Akerman, N. Navon, S. Kotler, Y. Glickman, and R. Ozeri, *New Journal of Physics* **17**, 113060.